Monomer Adsorption of Indocyanine Green to Gold Nanoparticles

Luca Guerrini,*[a,b] Liesbeth Hartsuiker[b], Srirang Manohar[c] and Cees Otto[*b]

[a] *Instituto de Estructura de la Materia, Consejo Superior de Investigaciones Científicas, Serrano, 121. 28006, Madrid, Spain. Tel. +34 91 561 6800; Fax. +34 91 564 5557; E-mail: lucaguerrini@cfmac.csic.es*

[b] *University of Twente, Faculty of Science and Technology, Medical Cell BioPhysics, MIRA Institute for Biomedical Technology and Technical Medicine, Postbus 217, 7500 AE Enschede, The Netherlands. Fax: +31 53 489 3511; Tel: +31 53 489 3159; E-mail: c.otto@utwente.nl*

[c] *University of Twente, Faculty of Science and Technology, BioMedical Photonic Imaging, MIRA Institute for Biomedical Technology and Technical Medicine, Postbus 217, 7500 AE Enschede, The Netherlands.*

Abstract

NIR-dye encoded gold nanoparticles (GNP) are rapidly emerging as contrast agents in many bio-imaging/sensing applications. The coding process is usually carried out without control or a clear understanding of the metal-liquid interface properties which, on the contrary, are critical in determining the type and extension of dye-metal interaction. In this paper, we investigated the effect of gold surface composition on the adsorption of Indocyanine Green (ICG) on GNP, simulating the surface conditions of gold nanorods on citrate-capped gold nanospheres. These substrates allowed a careful control of the metal-liquid interface composition and, thus, detailed absorption - and fluorescence concentration studies of the effects of each individual chemical in the colloidal solution (i.e. bromide anions, Cetyl trimethylammonium ions and Ag^{+}-ions) on the ICG-gold interaction. This study reveals the drastic effect that these experimental parameters can have on the ICG adsorption on GNP.

Introduction

ICG is a water-soluble, amphiphilic tricarbocyanine near-infrared emitting dye, which is approved by the Food and Drug Administration (FDA) for *in vivo* applications. Currently, ICG is used extensively as a marker in clinical imaging applications [1-4] with a major role in the detection of tumor metastases. For example, ICG is applied in intra-operative surgery to detect the sentinel lymph nodes of, for example, breast cancer, gastric cancer and colon cancer.[5-7]

In this field of *in vivo* cell and tissue targeting, gold nanoparticles (GNP) are rapidly emerging as contrast agents. GNP need to be functionalized with various (bio)chemicals for different applications. For bio-imaging and sensing they are usually coded with NIR dye reporters,[8, 9] such as indocyanine green (ICG). However, the coding process is not a trivial issue, as the metal-liquid interface composition plays a key role in determining the type of interaction and the extent of analyte adsorption on the GNP.[10] Nevertheless, labelling gold surfaces is usually carried out by simple addition of dye molecules to a GNP suspension without control or a clear understanding of the interface properties which affect the dye tagging of the nanomaterial.

Among GNP, gold nanospheres have been the most employed so far because the synthesis of monodisperse colloidal populations in a wide range of diameters (1.5-100 nm) is relatively easy and well-controllable.[11] However, their optical properties are poorly tunable in that their strong plasmon peak remains in the neighbourhood of 520 nm in the green region. This restricts their use in tissue as light penetration in this wavelength region is low. Recently, a large number of different nanostructures have become available which have unique plasmonic signatures in the far/red and near/infrared (NIR) regions, the so/called “biomedical window” of tissue, where light penetration is improved.

Structures such as nanoprisms, nanobars, nanoplates, nanocubes, nanorice and star-shaped GNP have been produced.[12-18] Of these, gold nanorods (GNR) have attracted enormous attention due to the relative ease with they can be synthesized with an exquisite control of their plasmon peaks and are being actively investigated for medical applications in (bio)chemical sensing and imaging, drug delivery and cancer therapy. [19-24]

In this paper, we aim to systematically investigate the effect of gold surface composition on the adsorption of ICG, in order to acquire insights of the roles played by each experimental factor on the coding process of the nanostructure. Specifically, we simulated GNR surface conditions on citrate-capped gold nanospheres. These substrates allowed a careful control of the metal-liquid interface composition and, thus, detailed absorption - and fluorescence concentration studies of the effects of each individual chemical in the colloidal solution (i.e. bromide anions, Cetyl trimethylammonium ions and Ag^+-ions) on the ICG-gold interaction. Such investigations are more complex on GNR, because of their more involved synthesis [25-29] and high susceptibility to aggregation and reshaping upon surface reactions.[30-32]

GNR of different size and aspect ratios are grown from seed gold nanospheres in the presence of CTA^+Br^- (CTAB), which acts as surface directing agent.[21, 33] CTAB regulates the shape of the GNR by forming densely packed CTA^+ bilayers on specific facets on gold surfaces, directing gold deposition to other facets, which contributes to the anisotropic growth of gold nanocrystals.[30, 34, 35] The bromide counterion plays an important role in nanorod formation. [25] Furthermore, Ag^+ is commonly added to the growth mixture to generate higher yields of rod-shaped gold nanoparticles with controllable aspect ratios.[33-35]

Since gold nanostructures quench the fluorescence of dye molecules in close proximity to the metal surface,[36] fluorescence spectroscopy directly informs about the ICG monomer population in the bulk solution. On the other hand, absorption measurements provide qualitative and quantitative information about the overall populations of both ICG monomer and dimer in the GNP suspensions. The amphiphilic character of ICG results in reversible self-organization into highly ordered aggregates upon an increase in concentration, predominantly caused by van der Waals forces and hydrophobic interactions.[37-39] The organization of ICG in dimers, oligomers and higher order aggregates is accompanied by changes in optical properties, which allows complementary information to be gathered from different spectroscopic techniques.

Here, we demonstrate that changes in relative CTAB concentration and presence of Ag^+ may have a dramatic effect on the ICG adsorption on the gold substrate. This points out that careful control of these parameters is crucial for the effective labeling of the nanostructure. Based on our results, we propose a model describing the dynamics of ICG adsorption to the gold surface in relation to the dye monomer-dimer equilibrium in the bulk solution.

Results and discussion

ICG adsorption on GNP

Figure 1A shows the ICG absorption spectrum in aqueous salt solution that roughly reproduces the ionic strength and pH of GNP colloid. Figure 1A illustrates the reversible self-organisation into dimers upon a concentration increase as a result of ICG's amphiphilic character.[37-39] At low dye concentration ($\leq 10^{-7}$ M) the mole fraction of dimers is negligible [37] and the absorption profile is dominated by the band at ~ 780 nm. An increase of the dye concentration to the range of 10^{-7}-10^{-4} M results in dimer formation and a relative intensity increase of the feature at ~ 705 nm. [33] The progressive

shift of the M↔D equilibrium towards the dimer form upon an increase in dye concentration is represented in Figure 1B (black squares), by plotting the absorption ratio at ~780 nm (H_{780}) and ~705 nm (H_{705}) against the ICG concentration in logarithmic scale.

Figure 2A shows the fluorescence emission of ICG $3x10^{-6}$ M in salt solution (black line). Fluorescence intensity of ICG in salt solution initially increases with the ICG concentration (Figure 2B, black squares) reaching a maximum fluorescence at ~ $5x10^{-6}$ M. At higher concentrations, quenching of the fluorescence emission signal occurs, due to the formation of ICG dimers and larger aggregates.[45] In the presence of Citrate/GNP, fluorescence emission decreases for ICG concentration below ~ 10^{-5} M, and the maximum fluorescence intensity shifts towards higher ICG concentrations (Figure 2B, green stars).

The quenching effect is more pronounced for Br/GNP (Figure 2, red).

This is consistent with the preferential adsorption of monomer ICG on the metal surface, whose fluorescence emission is then subsequently quenched via an increased non-radiative relaxation of the excited state due to energy and/or electron transfer with the plasmonic nanostructures. [36] This conclusion is further supported by the data shown in Figure 1B, since the adsorption of ICG monomers at the Br/GNP surface shifts the M↔D equilibrium in solution towards monomers suggesting an overall increase of monomer populations at the expense of dimers. However, it is not possible from absorbance and fluorescence spectra alone to determine potential self-assembly of monomers after adsorption on the GNP surface.

Addition of silver ions to Br/GNP solutions shifts the maximum of the fluorescence emission to even higher concentrations (ICG < ~$3x10^{-5}$ M, Figure 2B, blue triangles), which indicates that Ag^+ deposition on the gold surface provides a more effective adsorption of monomer ICG to gold nanoparticles. For dye concentrations larger than ~$3x10^{-5}$ M, the fluorescence intensity of ICG-GNP solutions converges to similar values as for ICG in salt solution indicating that dimer formation is no longer affected by the presence of GNP. These data are in excellent agreement with the data from absorption spectroscopy in Figure 1B.

Furthermore, it can be noted that a high ICG concentration does not induce GNP aggregation (Figure S3 of the ESI†), which is advantageous for the potential use of ICG as a GNP marker, as other fluorescent dyes show a tendency to produce GNP aggregation at high surface coverage.[46, 47]

Like other organic molecules [48, 49], ICG possesses in its structure a positively charged aromatic nitrogen atom in the benzo[e]indole ring which has a high tendency to interact with the metal NP through Coulomb interaction with previously adsorbed halide anions such as Cl^-, Br^- and I^-, which are known to adsorbs strongly on gold and silver surfaces [36, 50]. Therefore, we suggest that ICG interacts with the gold surface via binding with residual chloride anions from the GNP synthesis (in the case of Citrate/GNP) or with the larger number of bromide anions added *a posteriori* to the colloid (Br/GNP). Moreover, in a recent paper, Sanchez-Cortes and co-workers demonstrated the self-adsorption of Ag^+ ions on GNP surfaces with the formation of strong Ag^+-Cl^- bonds and consequential marked alteration of the electronic properties of the halide anions at the metal surface. [51] Accordingly, we can ascribe the drastic increase of ICG adsorption on Br/Ag/GNP surfaces to the improved electron donor ability of bromide anions resulting from their interaction with self-assembled Ag^+ ions onto the gold surface.

The previous results support the notion that monomer ICG preferentially adsorbs to GNP, effectively shifting the well-known monomer-to-dimer equilibrium of ICG in aqueous solution to the monomer state. In Figure 3A and 3B the adsorption behaviour of ICG onto gold nanoparticles in the presence of Br^- (Figure 3A) and Br^- and Ag^+-ions (Figure 3B) has been outlined for relevant ranges of the concentration of ICG. The relations between monomers M and dimers D are described, both in the bulk solution and with respect to the corresponding situation in aqueous solutions (no GNP).

At a dye concentration below $8x10^{-6}$ M, (Figure 3A, pane (1)), the mole fraction of ICG dimers in solution is negligible ($[M_b]>>[D_b]$). The adsorption of ICG monomers on the Br/GNP surface (M_s) and the subsequent quenching of the fluorescence emission lead to a proportional decrease of the fluorescence intensity as compared to ICG in aqueous solution (Figure 2B) in the absence of GNP.

At an intermediate concentration of ~$8x10^{-6}$ M, (Figure 3A(2)), the dimer population of ICG becomes more relevant as the ICG state in solution has to be described by the $M_b \leftrightarrow D_b$ equilibrium. As a result, a loss in $[M_b]$, caused by the adsorption of ICG on the Br/GNP, is counterbalanced by a shift of the $M_b \leftrightarrow D_b$ equilibrium toward the monomer state (Figure 2B). This effect leads to an appreciable increase of the H_{780}/H_{705} ratio towards higher ICG concentrations with respect to aqueous solution in Figure 1B.

The presence of silver ions drastically enhances monomer ICG adsorption as indicated by the complete quenching of dye fluorescence up to a [ICG] concentration of ~$8x10^{-6}$ M. The concentration of GNP is 0.29 nM and the onset of fluorescence emission in the presence of Br/Ag/GNP is therefore consistent with a full surface coverage of GNP (Figure 3B(2)). As a direct consequence, silver deposition also increases the minimally required dye concentration to observe dimer formation in the bulk solution (Figure 3B(3)).

The GNP-induced shift in the monomer-dimer equilibrium cannot be detected when the ICG concentration is raised above ~$1.5x10^{-5}$ M (Figure 3A and B(3)), because at elevated concentrations the dimer population becomes dominant in the bulk. In fact, a high D_b concentration maintains an approximately constant monomer concentration in the bulk, roughly independent of the fraction of dye molecules M_s adsorbed to the GNP surface. Consequentially the effect of silver ions on the $M_b \leftrightarrow D_b$ equilibrium is limited (Figure 3B(4)).

Accordingly, the $M_b \leftrightarrow D_b$ equilibrium is hardly influenced by the presence of GNP, either in the absence or the presence of silver once full surface coverage is achieved upon a further increase in ICG concentration, over ~$3x10^{-5}$ M (Figure 3(4)). The dimer population becomes dominant and unspecific physical multilayer deposition cannot be discarded, i.e. both monomers and dimers from the aqueous solution may adsorb onto the dye covered surface. As a result, both H_{780}/H_{705} and fluorescence and data converge to the values observed for ICG in salt solution (Figures 1B and 2B).

Effect of CTAB

CTAB plays a key role in the production of many different morphologies of gold nanoparticles. The production of gold nanospheres does not require CTAB and the concentration of CTAB can therefore be adjusted at will. ICG is known to incorporate into the interface of CTAB micellar structures, which affects its optical properties.[37]

Figure 4 shows that the concentration of unbound CTAB in aqueous solutions strongly modifies the aggregation states of ICG whereas, in this case, the effect of GNP appears marginal (Figure S4 of the ESI†). In Figure 4A, the peak height ratio H_{780}/H_{705} calculated from absorption spectra of ICG dissolved in CTAB solutions at different concentrations is plotted against the ICG/CTAB concentration ratio. The corresponding absorption spectra of $3x10^{-5}$ M ICG in aqueous solutions with different CTAB concentrations are shown in Figure 4B.

Above the critical micelle concentration (cmc) of ~1.2 mM for CTAB, [52, 53] the dye molecules are highly stabilized as monomer encapsulated in CTAB micelles,[4] referred to as M* (red, trace a). Micellar encapsulation of ICG reduces the formation of dye dimers and higher-order aggregates, [4] leading to an absorption spectrum dominated by monomeric responses (Figure 4B(a)). In addition, ICG micellar encapsulation also results in an up-shift of ~10-25 nm for absorption maxima, for both monomers and dimers, as compared to the spectrum of the dye in water (Figure 1A). [37]

However, when the CTAB concentration is decreased to just below the cmc value, ICG molecules form dimers (D*) even at very low dye concentrations (blue, trace b). Thus, CTAB affects ICG dimerisation in aqueous environments. When the CTAB concentration is further decreased, a sudden change of the optical properties of ICG occurs (green, trace c). This change indicates a transition from the highly dimerised state in a CTAB environment (blue, trace b) to a state reflecting the dye molecules in a water-like surrounding (yellow, trace d). This transition takes place for [CTAB] ~ [ICG] and shows a broad absorption at ~ 820 nm (Figure 4B(c)), which we propose to be attributed to an intermediate form, labelled as I*. This marked red-shift of the absorption maximum may suggest the formation of larger ordered aggregates, similar to those reported for J-aggregates. [39, 40]

Conclusions

Citrate-capped spherical gold nanoparticles were chosen as an experimental model for the interaction of gold nanoparticle surfaces with the medical contrast agent ICG. Since spherical gold nanoparticles do not require either Ag^+ or CTAB during synthesis, addition of these compounds in varying concentrations offers an opportunity to investigate the potential role of Ag^+ and CTAB on the adsorption of ICG. ICG adsorption to gold nanoparticles and the effect of the presence of Ag^+ and CTAB on the ICG adsorption was studied with fluorescence emission and UV-Vis absorption spectroscopy. Fluorescence emission of ICG adsorbed to gold is quenched,[36, 45] and the absorption spectra provide quantitative information about the overall monomer and dimer populations in solution and colloidal suspensions.

ICG in aqueous solution exists in equilibrium between monomers, dimers and higher-order aggregates. The fluorescence emission data as well as the absorption data show that the presence of gold nanospheres shifts the equilibrium to increased monomer contribution. This result suggests that monomeric ICG exhibits higher affinity to the gold surface as compared to the dimer. The observed ICG adsorption is summarized in Figure 3 for the relevant range of concentrations for which the existence of monomer-dimer equilibrium is noticeable. Additional Ag^+ deposition on GNP leads to an overall increase

in ICG adsorption on the metal surface, as a result of a drastic strengthening of the dye-metal interaction.

CTAB, which is an essential component in gold nanorod production and production of other gold nanoparticle geometries, affects the adsorption of ICG to gold nanoparticles because CTAB micellar structures compete for the available ICG. In the presence of CTAB above the critical micellar concentration (cmc), ICG intercalates in the micelles, which prevents ICG adsorption onto GNP. When the surfactant concentration is decreased to just below the cmc value, the monomer-to-dimer ratio decreases, suggesting stabilization of ICG in the form of dimers. Thus, the unbound surfactant concentration in the colloidal suspension may dramatically modify the dye aggregation state in the mixture and, in turn, its affinity to the metal surface. In addition, as CTAB constantly exchanges from the GNP surrounding bilayer to the solution, the CTAB concentration in the bulk plays a key role in the release of the surfactant from the GNP.[54]

These results show that the ICG adsorption on the spherical gold nanoparticles can be very different even for slight changes in the experimental parameters, such as concentrations of ICG, CTAB and presence of Ag^+. Therefore, careful control of these variables is crucial for the effective dye labeling of gold nanostructures.

Experimental

All reagent grade chemicals were used as received. Milli-Q water was used throughout the experiments. Indocyanine Green (ICG) was purchased from Fluka. Gold(III) chloride hydrate ($HAuCl_4 \cdot nH_2O$) >99.9% was provided by Aldrich. Cetyltrimethylammonium bromide (CTAB) > 99% was obtained from Sigma. Silver Nitrate ($AgNO_3$) >99% was purchased from Sigma-Aldrich.

Fresh ICG solutions, from 10^{-5} M to 10^{-2} M, were prepared in methanol before every set of measurements. The photostability and thermal stability of ICG molecules in methanol is considerably higher than in water.[40] Besides, the tendency for ground state dimer formation is very weak in methanol, and ICG is predominantly present as a monomer up to a concentration of about $5x10^{-2}$ M.[41] In this way, ICG molecules were always added as monomers to different samples, independently of the stock solution concentration.

Aqueous salt solution contains sodium citrate ($5x10^{-4}$ M), hydrochloric acid ($5x10^{-4}$ M) and potassium bromide (10^{-3} M) and shows the same pH of the gold colloid (pH~6). ICG concentration-dependent behaviour was investigated in this salt solution instead of pure Milli-Q water in order to broadly reproduce the pH and ionic strength conditions of the GNP suspension after the addition of KBr. In fact, these two parameters slightly affect the distribution of ICG molecules in solution.[39] Stock CTAB solution (0.4 M) was prepared by dissolving the surfactant in Milli-Q water and then appropriately diluting to the desired concentration. The resulting mixtures were sonicated before experiment for ~20 min.

Citrate-capped gold nanoparticles (GNP)

Citrate-capped gold nanoparticles of ~ 15 nm diameter (0.29 nM [42]) were prepared by reduction of chloroauric acid with sodium citrate.[43] 0.1 mL of $HAuCl_4$ 0.118 M solution

was added to 50 mL of Milli-Q water. Then 1 mL of sodium citrate 0.0388 M solution was added under stirring. The mixture was boiled for 15 minutes under reflux.

Fresh ICG solutions, from 10^{-5} M to 10^{-2} M, were prepared in methanol before every set of measurements. The photostability and thermal stability of ICG molecules in methanol is considerably higher than in water.[47] Besides, the tendency for ground state dimer formation is very weak in methanol, and ICG is predominantly present as a monomer up to a concentration of about $5x10^{-2}$ M.[50] In this way, ICG molecules were always added as monomers to different samples, independently of the stock solution concentration.

Salt solution contains sodium citrate ($5x10^{-4}$ M), hydrochloric acid ($5x10^{-4}$ M) and potassium bromide (10^{-3} M) and shows the same pH of the gold colloid (pH~6). ICG concentration-dependent behaviour was investigated in this salt solution instead of pure Milli-Q water in order to broadly reproduce the pH and ionic strength conditions of the GNP suspension after the addition of KBr. In fact, these two parameters slightly affect the distribution of ICG molecules in solution.[40]

Br/GNP

By adding 20 μL of a KBr 0.05 M water solution to 1 mL of GNP suspension, Br/GNP were prepared. The final bromide concentration in the suspension is 10^{-3} M, which was selected as the optimum concentration to provide a large number of active sites for ICG adsorption but without inducing observable GNP aggregation in the experimental time-scale (Figure S1 of the ESI†).

Br/Ag/GNP

To an aqueous solution to 1 ml of Br/GNP colloid, 5 μL of $AgNO_3$ $1.5x10^{-2}$ M was added. CTA/Br/Ag/GNP samples were prepared as for CTA/Br/GNP except that 5 μL of $AgNO_3$ $1.5x10^{-2}$ M aqueous solution was added to 1 ml of Br/GNP colloid before the addition of CTAB 0.4 M solution.

CTA/Br/GNP

A large excess of CTAB (0.125 mL of CTAB 0.4 M) was mixed with 1 mL of GNP. CTAB-capped GNPs were centrifuged from one to three times to progressively decrease the surfactant concentration: (1) 1st centrifugation: 12K rpm, 30 min; (2) 2nd centrifugation: 12K rpm, 30 min; and (3) 3rd centrifugation: 12K rpm, 5 min or 20 min. We will refer to these systems as CTA/Br/GNP (1), (2) and (3), respectively. The first two centrifugations do not produce significant GNP aggregation as judged from the absorption spectra, whereas the third centrifugation step causes a profound aggregation regardless of the time of centrifugation (Figure S2 of the ESI†).

Instrumentation

Fluorescence spectra were measured with a Fluoromax-4 (Horiba Jobin Yvon) spectrofluorometer with the following set-up: excitation 780 nm, excitation slit 5 nm/emission slit 10 nm, applied voltage 700 V. Samples for UV-visible absorption spectroscopy were prepared in the same way as those for the corresponding emission spectra and were recorded in a Shimadzu UV-2401PC spectrophotometer.

Fluorescence and UV-Vis absorption measurements were performed on Citrate/GNP, Br/GNP, Br/Ag/GNP and CTAB solution by adding to 1 ml suspension different aliquots of ICG stock solutions up to the desired concentration. For both fluorescence and absorption measurements, samples were measured in 1ml polystyrene cuvettes (Plastibrand standard disposable cuvettes, Sigma-Aldrich).

The molecular footprint of ICG on GNP was calculated to be ~2.6 nm^2, as obtained from a geometrical optimization of the dye molecular structure in water using the Hartree-Fock method with the 6-31G(d) basis set, Gaussian 09 program. [44] Approximately 270 molecules of ICG may therefore be expected in the first monolayer of an individual GNP with a diameter of 15 nm.

Acknowledgements
This work has been supported by the COST Action MP0603 (Micro CARS) through a short term scientific mission (L.G.) and by the SenterNovem IOP Photonic Devices project PRESMITT (IPD067771): Plasmon resonant nanoparticles for molecular imaging and therapy of tumours: in vitro to preclinical studies (L.H.).

Notes
†Electronic Supplementary Information (ESI) available: [Additional details concerning the effects of bromide, CTAB and ICG concentration on GNP stability. ICG absorption spectra on CTAB/GNP]. See DOI: 10.1039/b000000x/

References

1. T. Tsubono, S. Todo, N. Jabbour, A. Mizoe, V. Warty, A. J. Demetris and T. E. Starzl, *Hepatology*, 1996, **24**, 1165-1171.
2. V. Ntziachristos, A. G. Yodh, M. Schnall and B. Chance, *Proceedings of the National Academy of Sciences of the United States of America*, 2000, **97**, 2767-2772.
3. K. Licha, B. Riefke, V. Ntziachristos, A. Becker, B. Chance and W. Semmler, *Photochemistry and Photobiology*, 2000, **72**, 392-398.
4. J. M. Devoisselle, S. Soulie, S. Mordon, T. Desmettre and H. Maillols, *Advances in Fluorescence Sensing Technology Iii*, 1997, **2980**, 453-460.
5. C. Hirche, D. Murawa, Z. Mohr, S. Kneif and M. Hunerbein, *Breast Cancer Res. Treat.*, 2010, **121**, 373-378.
6. Y. Tajima, K. Yamazaki, Y. Masuda, M. Kato, D. Yasuda, T. Aoki, T. Kato, M. Murakami, M. Miwa and M. Kusano, *Ann. Surg.*, 2009, **249**, 58-62.
7. M. van der Pas, G. van Dongen, F. Cailler, A. Pelegrin and W. Meijerink, *Surg. Endosc.*, 2010, **24**, 2182-2187.
8. J. Kneipp, H. Kneipp, W. L. Rice and K. Kneipp, *Anal. Chem.*, 2005, **77**, 2381-2385.
9. X. M. Qian, X. H. Peng, D. O. Ansari, Q. Yin-Goen, G. Z. Chen, D. M. Shin, L. Yang, A. N. Young, M. D. Wang and S. M. Nie, *Nature Biotechnology*, 2008, **26**, 83-90.
10. L. Guerrini, Z. Jurasekova, C. Domingo, M. Perez-Mendez, P. Leyton, M. Campos-Vallette, J. V. Garcia-Ramos and S. Sanchez-Cortes, *Plasmonics*, 2007, **2**, 147-156.
11. M. C. Daniel and D. Astruc, *Chem. Rev.*, 2004, **104**, 293-346.
12. F. Hao, C. L. Nehl, J. H. Hafner and P. Nordlander, *Nano Lett.*, 2007, **7**, 729-732.
13. N. R. Jana, *Angew. Chem.-Int. Edit.*, 2004, **43**, 1536-1540.
14. R. C. Jin, Y. W. Cao, C. A. Mirkin, K. L. Kelly, G. C. Schatz and J. G. Zheng, *Science*, 2001, **294**, 1901-1903.
15. J. S. Shumaker-Parry, H. Rochholz and M. Kreiter, *Adv. Mater.*, 2005, **17**, 2131-2138.
16. B. J. Wiley, Y. C. Chen, J. M. McLellan, Y. J. Xiong, Z. Y. Li, D. Ginger and Y. N. Xia, *Nano Lett.*, 2007, **7**, 1032-1036.
17. C. J. Murphy and N. R. Jana, *Adv. Mater.*, 2002, **14**, 80-82.
18. J. M. McLellan, Z. Y. Li, A. R. Siekkinen and Y. N. Xia, *Nano Lett.*, 2007, **7**, 1013-1017.
19. X. H. Huang, I. H. El-Sayed, W. Qian and M. A. El-Sayed, *J. Am. Chem. Soc.*, 2006, **128**, 2115-2120.
20. X. H. Huang, S. Neretina and M. A. El-Sayed, *Adv. Mater.*, 2009, **21**, 4880-4910.
21. J. Perez-Juste, I. Pastoriza-Santos, L. M. Liz-Marzan and P. Mulvaney, *Coordination Chemistry Reviews*, 2005, **249**, 1870-1901.
22. S. Abalde-Cela, P. Aldeanueva-Potel, C. Mateo-Mateo, L. Rodriguez-Lorenzo, R. A. Alvarez-Puebla and L. M. Liz-Marzan, *Journal of the Royal Society Interface*, 2010, **7**, S435-S450.
23. R. A. Alvarez-Puebla and L. M. Liz-Marzan, *Small*, 2010, **6**, 604-610.

24. R. G. Rayavarapu, W. Petersen, L. Hartsuiker, P. Chin, H. Janssen, F. W. B. van Leeuwen, C. Otto, S. Manohar and T. G. van Leeuwen, *Nanotechnology*, 2010, **21**.
25. K. T. Yong, Y. Sahoo, M. T. Swihart, P. M. Schneeberger and P. N. Prasad, *Topics in Catalysis*, 2008, **47**, 49-60.
26. D. K. Smith and B. A. Korgel, *Langmuir*, 2008, **24**, 644-649.
27. R. G. Rayavarapu, C. Ungureanu, P. Krystek, T. G. van Leeuwen and S. Manohar, *Langmuir*, 2010, **26**, 5050-5055.
28. N. J. Durr, T. Larson, D. K. Smith, B. A. Korgel, K. Sokolov and A. Ben-Yakar, *Nano Lett.*, 2007, **7**, 941-945.
29. J. X. Gao, C. M. Bender and C. J. Murphy, *Langmuir*, 2003, **19**, 9065-9070.
30. C. X. Yu, L. Varghese and J. Irudayaraj, *Langmuir*, 2007, **23**, 9114-9119.
31. H. Takahashi, Y. Niidome, T. Niidome, K. Kaneko, H. Kawasaki and S. Yamada, *Langmuir*, 2006, **22**, 2-5.
32. H. Ding, K. T. Yong, I. Roy, H. E. Pudavar, W. C. Law, E. J. Bergey and P. N. Prasad, *J. Phys. Chem. C*, 2007, **111**, 12552-12557.
33. B. Nikoobakht and M. A. El-Sayed, *Chemistry of Materials*, 2003, **15**, 1957-1962.
34. N. R. Jana, L. Gearheart and C. J. Murphy, *Chemistry of Materials*, 2001, **13**, 2313-2322.
35. R. Rayavarapu, W. Petersen, C. Ungureanu, J. Post, T. van Leeuwen and S. Manohar, *International Journal of Biomedical Imaging*, 2007, **Article ID 29817**.
36. E. C. Le Ru and P. G. Etchegoin, *Principles of Surface-Enhanced Raman Spectroscopy*, Elsevier, 2009.
37. K. Kirchherr, A. Briel and K. Mader, *Molecular Pharmaceutics*, 2009, **6**, 480-491.
38. M. L. J. Landsman, G. Kwant, G. A. Mook and W. G. Zijlstra, *Journal of Applied Physiology*, 1976, **40**, 575-583.
39. R. Weigand, F. Rotermund and A. Penzkofer, *J. Phys. Chem. A*, 1997, **101**, 7729-7734.
40. W. Holzer, M. Mauerer, A. Penzkofer, R. M. Szeimies, C. Abels, M. Landthaler and W. Baumler, *Journal of Photochemistry and Photobiology B-Biology*, 1998, **47**, 155-164.
41. R. Philip, A. Penzkofer, W. Baumler, R. M. Szeimies and C. Abels, *Journal of Photochemistry and Photobiology a-Chemistry*, 1996, **96**, 137-148.
42. X. O. Liu, M. Atwater, J. H. Wang and Q. Huo, *Colloid Surf. B-Biointerfaces*, 2007, **58**, 3-7.
43. G. Frens, *Nature-Physical Science*, 1973, **241**, 20-22.
44. M. J. Frisch, G. W. Trucks, H. B. Schlegel, G. E. Scuseria, M. A. Robb, J. R. Cheeseman, G. Scalmani, V. Barone, B. Mennucci, G. A. Petersson, H. Nakatsuji, M. Caricato, X. Li, H. P. Hratchian, A. F. Izmaylov, J. Bloino, G. Zheng, J. L. Sonnenberg, M. Hada, M. Ehara, K. Toyota, R. Fukuda, J. Hasegawa, M. Ishida, T. Nakajima, Y. Honda, O. Kitao, H. Nakai, T. Vreven, J. Montgomery, J. A.;, J. E. Peralta, F. Ogliaro, M. Bearpark, J. J. Heyd, E. Brothers, K. N. Kudin, V. N. Staroverov, R. Kobayashi, J. Normand, K. Raghavachari, A. Rendell, J. C. Burant, S. S. Iyengar, J. Tomasi, M. Cossi, N. Rega, N. J. Millam, M. Klene, J. E. Knox, J. B. Cross, V. Bakken, C. Adamo, J. Jaramillo, R. Gomperts, R. E.

Stratmann, O. Yazyev, A. J. Austin, R. Cammi, C. Pomelli, J. W. Ochterski, R. L. Martin, K. Morokuma, V. G. Zakrzewski, G. A. Voth, P. Salvador, J. J. Dannenberg, S. Dapprich, A. D. Daniels, Ö. Farkas, J. B. Foresman, J. V. Ortiz, J. Cioslowski and D. J. Fox, Gaussian, Inc.: Wallingford CT, Revision A.1 edn., 2009.
45. R. Rajagopalan, P. Uetrecht, J. E. Bugaj, S. A. Achilefu and R. B. Dorshow, *Photochemistry and Photobiology*, 2000, **71**, 347-350.
46. N. Narband, M. Uppal, C. W. Dunnill, G. Hyett, M. Wilson and I. P. Parkin, *Phys. Chem. Chem. Phys.*, 2009, **11**, 10513-10518.
47. L. O. Brown and S. K. Doorn, *Langmuir*, 2008, **24**, 2178-2185.
48. J. I. Millan, J. V. Garcia-Ramos, S. Sanchez-Cortes and R. Rodriguez-Amaro, *J. Raman Spectrosc.*, 2003, **34**, 227-233.
49. M. R. Lopez-Ramirez, L. Guerrini, J. V. Garcia-Ramos and S. Sanchez-Cortes, *Vibrational Spectroscopy*, 2008, **48**, 58-64.
50. H. Wetzel and H. Gerischer, *Chem. Phys. Lett.*, 1980, **76**, 460-464.
51. L. Guerrini, J. V. Garcia-Ramos, C. Domingo and S. Sanchez-Cortes, *J. Raman Spectrosc.*, 2010, **41**, 508-515.
52. M. A. Bahri, M. Hoebeke, A. Grammenos, L. Delanaye, N. Vandewalle and A. Seret, *Colloid Surf. A-Physicochem. Eng. Asp.*, 2006, **290**, 206-212.
53. M. Tedeschi, L. Franco, M. Ruzzi, L. Paduano, C. Corvaja and G. D'Errico, *Phys. Chem. Chem. Phys.*, 2003, **5**, 4204-4209.
54. J. Alper, M. Crespo and K. Hamad-Schifferli, *J. Phys. Chem. C*, 2009, **113**, 5967-5973.

Figure 1. Self-organisation from ICG monomers into dimers upon increase in ICG concentration. [A] Concentration-dependent absorption spectra of ICG in salt solution; from the top to the bottom, [ICG] = $7x10^{-5}$ M, $5x10^{-5}$ M, $3x10^{-5}$ M, $2x10^{-5}$ M, $1.5x10^{-5}$ M, $1x10^{-5}$ M, $7x10^{-6}$ M, $5x10^{-6}$ M, $3x10^{-6}$ M, $1x10^{-6}$ M, $7x10^{-7}$ M and $5x10^{-7}$ M. [B] Experimental values of the spectral parameter H_{780}/H_{705} at different dye concentration for ICG dissolved in salt solution, Br/GNPs and Br/Ag/GNPs colloids.

Figure 2. [A] Fluorescence spectra of ICG $3x10^{-6}$ M and [B] fluorescence intensity (logarithmic value) vs. ICG concentration, for dye molecules dissolved in salt solution, Citrate/GNP, Br/GNP and Br/Ag/GNP colloids. Excitation wavelength was 780 nm, fluorescence intensity was determined at the maximum of the fluorescence peak (ca. 820 nm) for monomeric ICG.

Figure 3. ICG adsorption scheme on [A] Br/GNP and [B] Br/Ag/GNP surfaces at different dye concentration. Monomer is labelled M, dimer D. The subscripts indicate: b for "bulk", referring to M and D existing in the bulk aqueous solution; s for "surface", referring to M chemisorbed on the gold surface. Mm and Dm stand for "multilayer", which refers to M and D physisorbed on the first ICG layer surrounding the GNP. Msalt stands for monomer dye molecules in pure aqueous solution (no GNP). The overall monomer population in the colloidal suspension is indicated as MTOT (=Mb + Ms).

Figure 4. [A] Experimental values of the spectral parameter H_{780}/H_{705} for ICG at different concentration in CTAB solutions (5000 μM, 500 μM, 50 μM and 5 μM) against [ICG]/[CTAB] ratio (logarithmic scale). [B] Absorption spectra of ICG $3x10^{-5}$ M in CTAB aqueous solutions at different surfactant concentration: (a) 5000 μM, (b) 500 μM and (d) 5 μM. (c) Absorption spectrum of ICG $3.7x10^{-5}$ M in CTAB aqueous solution 50 μM.

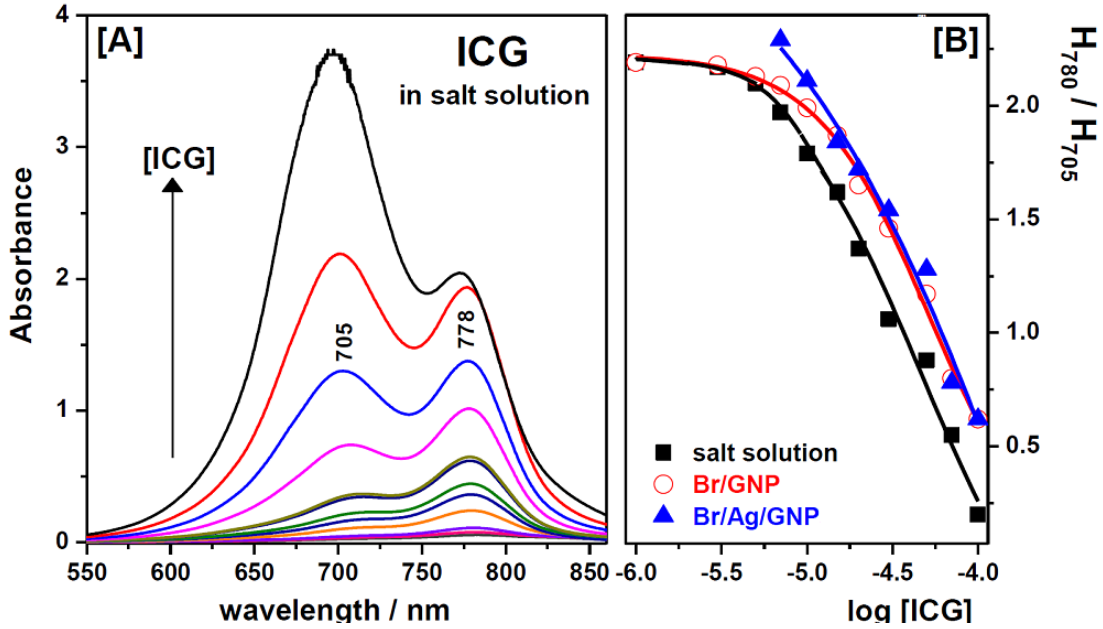
[A]
ICG
in salt solution
[ICG]
Absorbance
705
778
wavelength / nm
[B]
salt solution
Br/GNP
Br/Ag/GNP
log [ICG]
H780 / H705

Figure 1

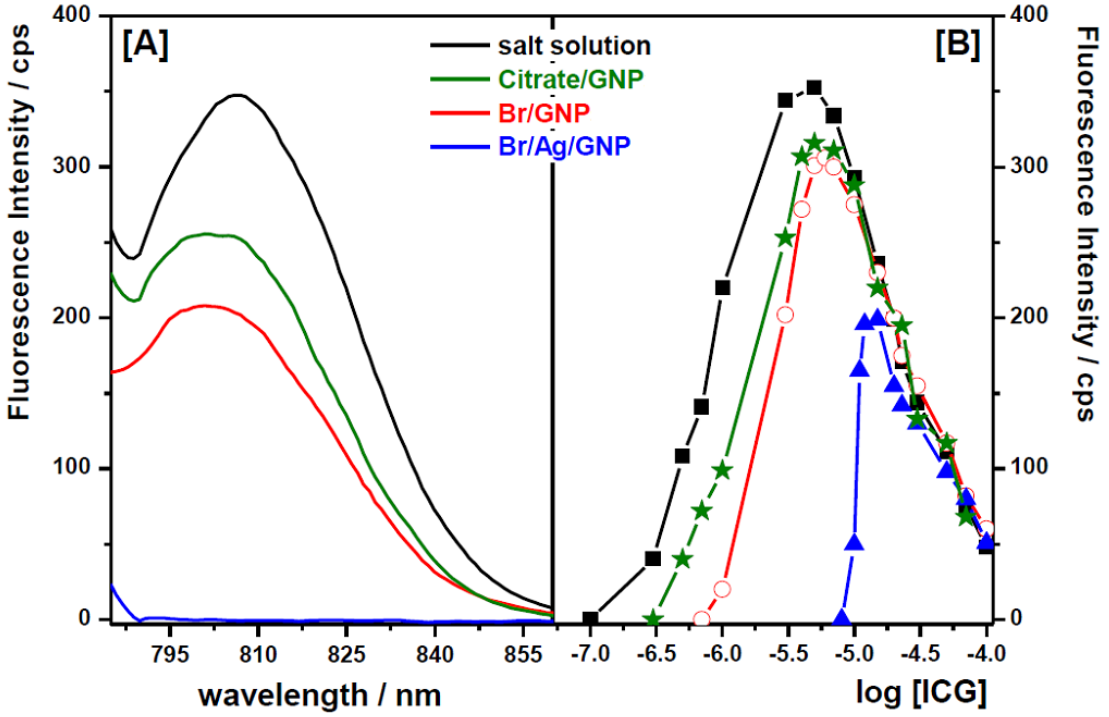
[A]
[B]
salt solution
Citrate/GNP
Br/GNP
Br/Ag/GNP
Fluorescence Intensity / cps
Fluorescence Intensity / cps
wavelength / nm
log [ICG]
400
300
200
100
0
795
810
825
840
855
-7.0
-6.5
-6.0
-5.5
-5.0
-4.5
-4.0

Figure 2

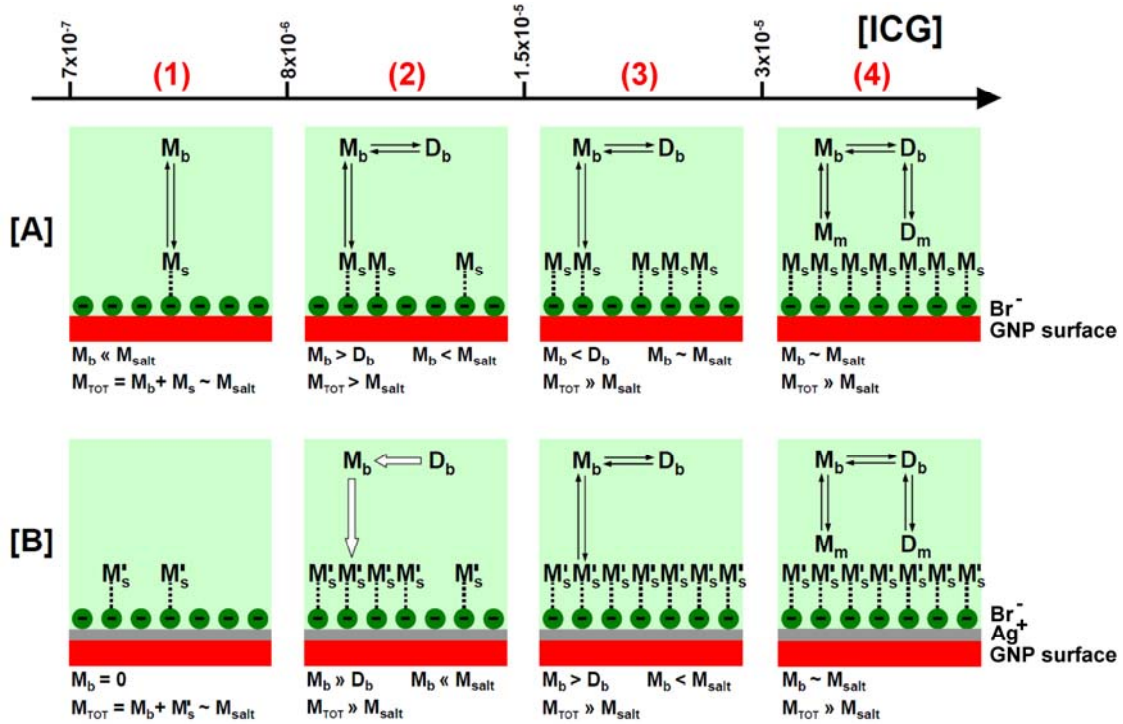
[ICG]
7x10-7
8x10-6
1.5x10-5
3x10-5
(1)
(2)
(3)
(4)
[A]
[B]
Mb
Ms
Db
Dm
M's
Br-
Ag+
GNP surface
Mb « Msalt
MTOT = Mb+ Ms ~ Msalt
Mb > Db
Mb < Msalt
MTOT > Msalt
Mb < Db
Mb ~ Msalt
MTOT » Msalt
Mb ~ Msalt
MTOT » Msalt
Mb = 0
MTOT = Mb+ M's ~ Msalt
Mb » Db
Mb « Msalt
MTOT » Msalt
Mb > Db
Mb < Msalt
MTOT » Msalt
Mb ~ Msalt
MTOT » Msalt

Figure 3

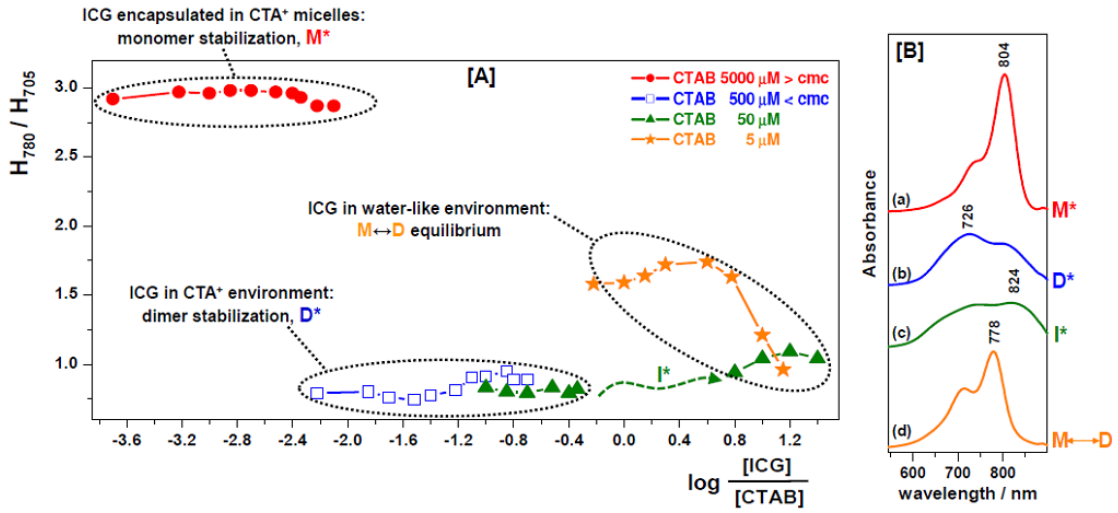
ICG encapsulated in CTA+ micelles:
monomer stabilization, M*
[A]
CTAB 5000 μM > cmc
CTAB 500 μM < cmc
CTAB 50 μM
CTAB 5 μM
ICG in water-like environment:
M↔D equilibrium
ICG in CTA+ environment:
dimer stabilization, D*
I*
H780 / H705
log [ICG]/[CTAB]
[B]
804
726
824
778
(a)
(b)
(c)
(d)
M*
D*
I*
M↔D
Absorbance
600 700 800
wavelength / nm

Figure 4